International Journal of Mechanical Sciences 53 (2011) 1–10

Contents lists available at ScienceDirect

International Journal of Mechanical Sciences

journal homepage: www.elsevier.com/locate/ijmecsci

The coupled vibration in a rotating multi-disk rotor system

Yi-Jui Chiu [a], Dar-Zen Chen [b,*]

[a] The Faculty of Mechanical Engineering and Mechanics, Ningbo University, No. 818, Fenghue Road, Ningbo, 315211 Zhejiang Province, China
[b] Department of Mechanical Engineering, National Taiwan University, No. 1, Sec. 4, Roosevelt Road, Taipei 10617, Taiwan, ROC

ARTICLE INFO

Article history:
Received 26 May 2010
Received in revised form
3 October 2010
Accepted 11 October 2010
Available online 27 October 2010

Keywords:
Multi-disk
Coupled vibration

ABSTRACT

The influence on coupling vibrations among shaft-torsion and blade-bending coupling vibrations of a multi-disk rotor system was investigated analytically. The natural frequencies and the mode shapes of the system were solved for one- to three-disk cases as examples. First, numerical results showed how the natural frequencies varied with blades in a disk unit. The diagrams of the coupling mode shapes were drawn. From the results, it was found that the inter-blade (BB) modes were of repeated frequencies of $(N_b\text{-}1)$ multiplicity for number blades. At multi-disk unit, the shaft–blade (SB) modes added to N_d modes for number disks. The BB modes were of repeated frequencies of $[N_d \times (N_b\text{-}1)]$ multiplicity for number disks. Numerical calculations also revealed that the natural frequencies were affected by disk distance. In the rotation effect, the times of instability will due to the number of disk. And, the more disk rotor causes instability earlier than the less disk case.

1. Introduction

The rotor systems composed of shaft, disk, and blades have been extensively implemented in the industry. The demands for higher operational speeds require more precise tuning than usual. The dynamics of rotor systems have been studied for several decades.

Investigations were confined to analyses of individual components, such as blade, Bauer [1] practiced the assumed modes method to investigate the vibrational behavior of a beam rotating with a constant spin about its longitudinal axis. Kammer and Schlack [2,3] utilized the perturbation method to study dynamic characteristics and stability of a rotating Euler beam. In last decades [4–9], many authors have reported new formulations and techniques for the rotating blade. On the other hand, about disks, Shen [10] further employed Rayleigh dissipation function and Lagrange's equation to solve for the forced responses of a rotating disk system. Shen and Ku [11] applied Lagrange's equations and linearized equation of motion to explore the multiple disk system, and found the frequencies of the unbalanced modes were lower than those of disk's one-nodal-diameter modes. Lately, Khorasany and Hutton [12] explored dynamic characteristics and stability of a constraining spinning disk.

Combined systems, like the shaft–disks, Nevzat [13] adopted analytical method to explore the shaft–disk system. He found critical speeds of the 1st and 2nd modes, and verified those with experiments. Wu and Flowers [14] adopted the transfer matrix method to solve for the natural frequency and critical rotational speed of multiple disks.

In the disk–blades unit, Chun and Lee [15] used the assumed modes method to analyze the effects of disk flexibility on the vibrational modes of a flexible disk–blade rotor system. They obtained more efficiency and correct results, compared to finite element method. Omprakash and Ramamurti [16] applied Love and Kichhoff method to study the effects on the natural frequency due to the blade stagger angle and twist angle in a disk–blades system.

Some studies have addressed the dynamic influence onto the coupled vibrations of a shaft–disk–blade unit. Lesaffre et al. [17] used the energetic method to explore the dynamic stability of a flexible bladed rotor in the rotating frame. The authors found and highlighted an unstable phenomenon near the stator critical speed even in case of frictionless sliding. Huang and Ho [18] utilized the concept of structure synthesis for a shaft–disk–blade system. The system was divided into two subsystems, the shaft–disk and blades. The disk was assumed to be rigid and can transmit the motion between a shaft and blades. The results showed that there existed not only the shaft–blade coupled modes but also the inter-blades coupling modes. Yang and Huang [19–21] explored the disk flexibility in a rotating shaft–disk–blade system. They studied the free vibration and classified four types of coupling modes, shaft–blade (SB), shaft–disk–blade (SDB), disk–blade (DB), and blade–blade (BB). Huang et al. [22] used same method to show the damping effect and the vibration analysis of a shaft–disk–blade system with viscoelastic layers on blades. Chiu and Huang [23] used assumed mode method to analyze the shaft-torsion and blade-bending coupling vibrations of a rotor system, in which the blades were grouped with lacing wires. They found the SB modes are unaffected by the lacing wires. That was however for a disk case.

In this paper, the rigid disk was considered and the blade is assumed to be of Euler type with no stagger angle. The emphasis is in the coupling behavior between shaft-torsion and blade-bending. The frequencies and the corresponding mode shapes in the shaft–disk–blade system are derived and discussed. Second, the paper

* Corresponding author. Tel.: +886 2 33662723; fax: +886 2 23692178.
E-mail address: dzchen@ntu.edu.tw (D.-Z. Chen).

0020-7403/$ - see front matter © 2010 Elsevier Ltd. All rights reserved.
doi:10.1016/j.ijmecsci.2010.10.001

Nomenclature

$\boldsymbol{q}$	generalized vector
v_b	blade displacements with respect to the Y_2 axes
$\hat{v}_b$	blade displacements with respect to the Y_3 axis
V_i	ith mode shape of the blade
w_b	blade displacements with respect to the Z_2 axes
w_d	disk transverse displacement with respect to the Z_1 axis
W_i	ith mode shape of the disk
ϕ	shaft–disk torsional displacement relative to rotation frame
Φ_i	ith mode shape of the shaft–disk
ω	natural frequency
ω_{b1}	first nature frequency of single cantilever blade
Ω	rotational speed

Subscripts

$()_b$	blade
$()_d$	disk
$()_s$	shaft

intended to provide a qualitative and quantitative overview of a periodic rotor with multi-disk. At last, the effects of rotation on the changes of the rotor's natural frequencies were illustrated.

2. Theoretical analysis

A rotor system composed of shaft, multi-disk, and blades is shown in Fig. 1. The rotor contains a torsional shaft, rigid disks, and flexible blades fixed onto the outer edge of the disk. Z_{d1} is the first disk's distance, and d_1 is the distance between two disks. Energies of the system are first derived and the assumed mode method is employed to discretize the equations of motion.

The torsional energies associated with the shaft–disk are

$$T_s = \frac{1}{2}\int_0^{Ls} I_s\left(\frac{\partial\phi}{\partial t}+\Omega\right)^2 dZ + \frac{I_d}{2}\left(\frac{\partial\phi}{\partial t}+\Omega\right)^2\Big|_{Z=Z_d} \tag{1}$$

$$U_s = \frac{1}{2}\int_0^{Ls} G_sJ_s\left(\frac{\partial\phi}{\partial Z}\right)^2 dZ \tag{2}$$

where $\psi(Z,t)$ is the torsional displacement with respect to a constantly rotating (Ω) frame; L_s, I_s, and G_sJ_s denote the shaft's length, polar rotary inertia, and torsional rigidity, respectively. I_d is the disk's polar rotary inertia.

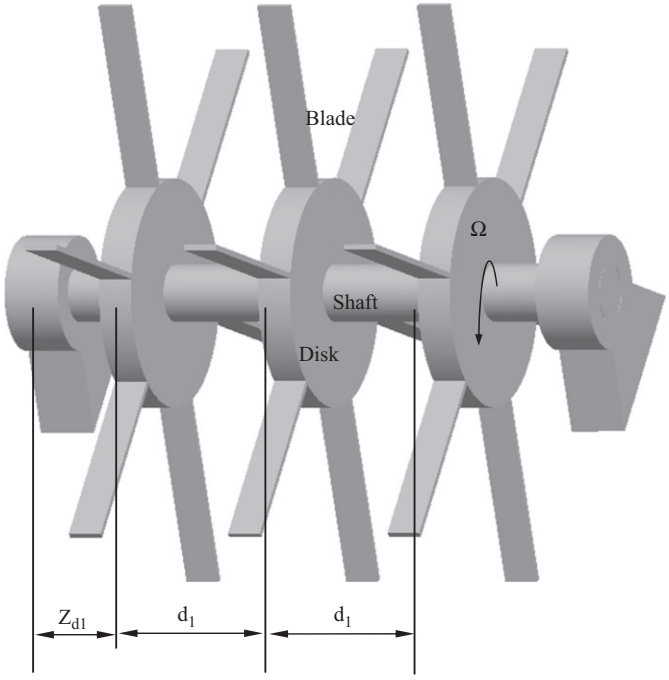

Fig. 1. A multi-disks rotor system.

Fig. 2 shows a typical rotating blade cantilevered onto a rigid disk. (X_1, Y_1, Z_1) coordinate system is the inertia frame, (x_2, y_2, z_2) frame rotates at a constant speed, and (x_3, y_3, z_3) frame is fixed to the blade's root.

The kinetic and strain energies associated with a blade are

$$T_b = \frac{1}{2}\int_{r_d}^{r_b}\rho_bA_b\left\{\left(\frac{\partial v_b}{\partial t}\right)^2+({v_b}^2+x^2)\Omega^2+2x\Omega\frac{\partial v_b}{\partial t}\right\}dx + \frac{1}{2}\int_{r_d}^{r_b} I_b\left(\Omega+\frac{\partial^2 v_b}{\partial x\partial t}\right)^2 dx \tag{3}$$

$$U_b = \frac{1}{2}\int_{r_d}^{r_b} E_bI_A\left(\frac{\partial^2 v_b}{\partial x^2}\right)^2 dx + \frac{1}{4}\int_{r_d}^{r_b}\rho_bA_b\Omega^2(r_b^2-x^2)\left(\frac{\partial v_b}{\partial x}\right)^2 dx \tag{4}$$

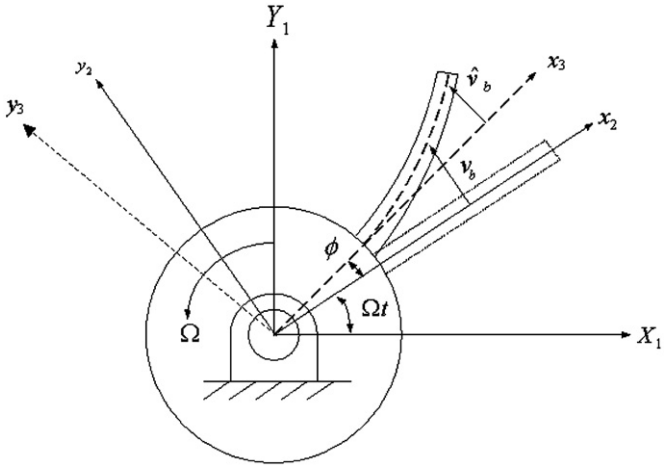

Fig. 2. Coordinate sets and deformation of a rotating blade.

Table 1
Geometric and material properties of the illustrated examples.

Shaft	
Density: ρ_s	7850 kg/m^3
Shear modulus: G_s	75 GPa
Shaft length: L_s	0.6 m
Radius: r_s	0.04 m
Disk	
Density: ρ_d	7850 kg/m^3
Location: z_d	0.3 m
Outer radius: r_d	0.2 m
Blade	
Density: ρ_b	7850 kg/m^3
Young's modulus: E_b	200 GPa
Blade outer end: r_b	0.4 m
Cross-section: A_b	1.2×10^{-4} m^2
Area moment of inertia: I_A	1.92×10^{-9} m^2
Rotational speed: Ω	0–2000 Hz

where v_b is the transverse displacements in y_2 direction. I_A is the area moment of inertia about the z_3 axis, and I_b is the polar moment of inertia. The displacement of the blade $v_b(x,t)$ consists of the shaft's torsional displacement $\phi(Z_d,t)$ and the blade's bending displacement $\hat{v}_b(x,t)$. The kinematic relations between these displacements are

$$v_b(x,t) = \hat{v}_b + x\phi\big|_{Z_d} \tag{5}$$

The assumed mode method is adopted to discretize the continuous system, i.e.,

$$\phi(Z,t) = \sum_{i=1}^{n_s} \Phi_i(Z)\eta_i(t) = \Phi(Z)\eta(t) \tag{6}$$

$$\hat{v}_{b_k}(x,t) = \sum_{i=1}^{n_b} V_i(x)\xi_{ik}(t) = \boldsymbol{V}(x), \quad k = 1,2,\ldots,N \tag{7}$$

Table 2
Natural frequencies (Hz) of shaft–disk and clamped blade.

Component's n.f.	ω_1	ω_2	ω_3
Shaft–disk (w/o blades)	207.418	2645.690	5267.204
Clamped blade (shaft–disk rigid)	81.538	510.99	1430.788

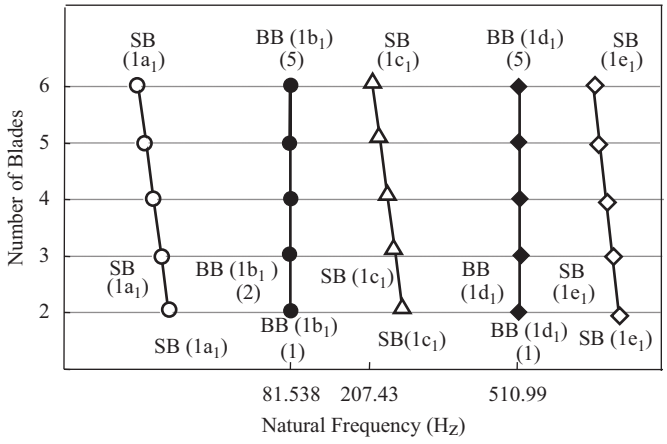

Fig. 3. Frequency changes due to blades in a two- to a six-blades rotor.

where Φ_i and V_i are the mode shapes of a torsional shaft and of a bending blade, respectively. These modes are chosen to be

$$\Phi_i(Z) = \sin\left[\frac{(2i-1)\pi Z}{2L_s}\right] \tag{8}$$

$$V_i(x) = (\sin\tau_i x - \sinh\tau_i x) + \alpha_i(\cos\tau_i x - \cosh\tau_i x) \tag{9}$$

is the beam function for blade with

$$[\cos\tau_i(r_b - r_d)][\cos h\tau_i(r_b - r_d)] + 1 = 0 \tag{10}$$

$$\alpha_i = \frac{-\sin\tau_i(r_b - r_d) - \sinh\tau_i(r_b - r_d)}{\cos\tau_i(r_b - r_d) + \cosh\tau_i(r_b - r_d)} \tag{11}$$

η_i and ξ_{ik} are the participation factors. n's with subscripts for the corresponding subsystems are the number of modes deemed necessary for required accuracy. In this study, the terms (n_s, n_b)=(7, 10) is enough to yield an accuracy up to 10^{-5} Hz.

Substitution of the above equations into the energy expressions and employment of the Lagrange equations yields the following discretizated equations of motion in matrix notation as:

$$[\mathrm{M}]\ddot{q} + ([\mathrm{K}^e] - \Omega^2[\mathrm{K}^\Omega]) = \mathbf{0} \tag{12}$$

where $[\mathrm{K}^e]$, arising from the elastic deflection, dominates at low rotational speed. The term $-\Omega^2[\mathrm{K}^\Omega]$, resulted from rotation, softens the rotor so that it becomes very significant at high rotational speed. It is also the major role affecting the stability of the rotor. The matrices [M], $[\mathrm{K}^e]$, and $[K^\Omega]$are given in Appendix A.

The matrices's dimensions are $(n_s+N_d\times N_b\times n_b)\times(n_s+N_d\times N_b\times n_b)$, where N_d and N_b are the number of disks and blades. $\boldsymbol{q}$ is a generalized vector, i.e.,

$$\boldsymbol{q} = \{\eta^T \backslash \xi_{11}^T \cdots \xi_{N_d1}^T \cdots \xi_{1N_b}^T \cdots \xi_{N_dN_b}^T\}^T \tag{13}$$

In the usual manner for free vibration analysis, it is assumed the solution is of the form $\boldsymbol{q}=\{c\}e^{\lambda t}$ with $\{c\}$ the undetermined coefficient vector and λ represents for the eigenvalue. Note that λ is a pure imaginary number for most of undamped rotors, i.e., $\lambda=i\omega$, $i=\sqrt{-1}$. Eq. (12) then yields to be

$$\{([K^e] - \Omega^2[K^\Omega]) + \lambda^2[M]\}\{c\} = \{0\} \tag{14}$$

The characteristic equation is

$$\left|([K^e] - \Omega^2[K^\Omega]) + \lambda^2[M]\right| = 0 \tag{15}$$

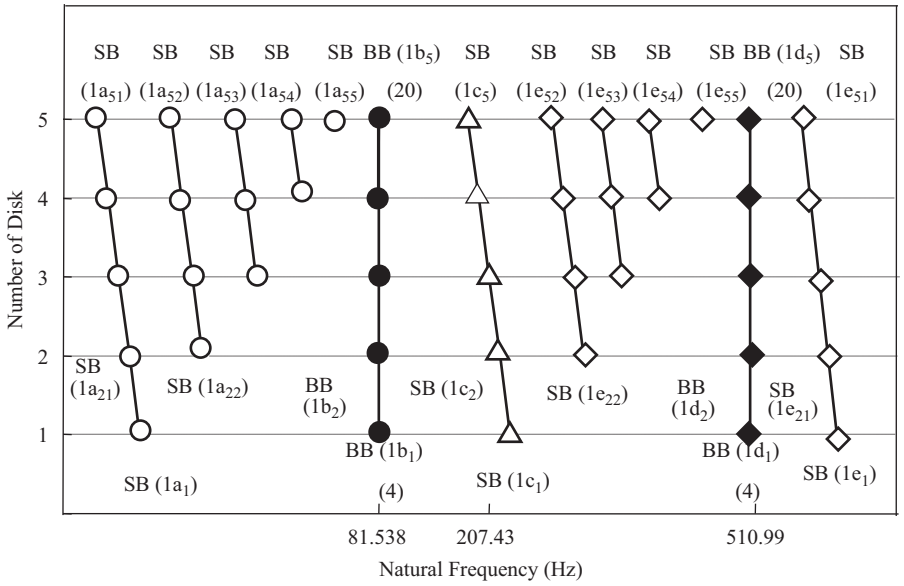

Fig. 4. Frequency changes due to disks in a five-blades rotor.

The mode shapes are solved for by first solving step for the eigenvalue from Eq. (15), then the eigenvectors from Eq. (12). Substitute the obtained eigenvalues and eigenvectors into Eqs. (6) and (7), then the mode shapes are sketched.

3. Numerical results

To be dimensional independent, the numerical results are normalized with respect to the disk's distance, therein, $d^* = d_1/Z_{d1}$. Table 1 lists the geometric and material properties of the illustrated examples. Note that, the length of blades is deliberately elongated in order to magnify the coupling behaviors. Table 2 provides a comparison basis for the effects of component on coupling vibration. These frequencies serve as validation and interpretation of the numerical results as well.

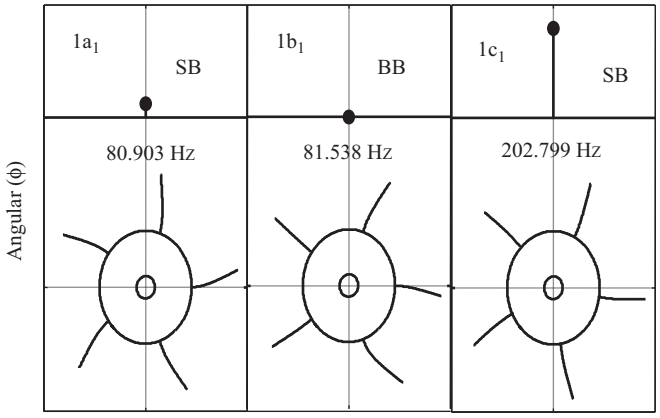

Fig. 5. The first three modes of the one-disk and five-blades rotor.

It is first of interest to realize how the blades affect the coupling vibrations. Fig. 3 shows the frequency changes for a two- to a six-blade system. $1a_1$ and $1b_1$ modes belong to a set where the blade's first mode predominates in a disk system. $1c_1$ mode belong to a set where the shaft's first mode predominates in a disk system. $1d_1$ and $1e_1$ modes belong to a set where the blade's second mode predominates in a disk system. Note that the abscissa, not drawn in a linear scale, has three reference marks at $\omega = 81.538$, 207.43 and 510.99, respectively, denoting the cantilevered blade's first bending, shaft's first torsion and the blade's second bending frequency (Table 1). For a disk system, the coupling modes could be grouped into two categories, including, the shaft–blade (SB) and blade–blade (BB). The BB modes were of repeated frequencies of $(N_b - 1)$ multiplicity for number blades.

Fig. 4 shows the frequency changes due to disks in a five-blades rotor. 1a and 1b modes belong to a set where the blade's first mode predominates in a multi-disk system. For a multi-disk system, the coupling modes also could be grouped into two categories, the shaft–blade (SB) and blade–blade (BB). Fig. 4 reveals a very significant phenomenon that the BB modes were of repeated frequencies of $[N_d \times (N_b - 1)]$ multiplicity for number disks. The shaft–blade (SB) modes where the blade's mode predominates were of frequencies of N_d for number disks. The shaft–blade (SB) modes where the shaft's mode predominates retained a mode, but the frequency reduced along with the disk number.

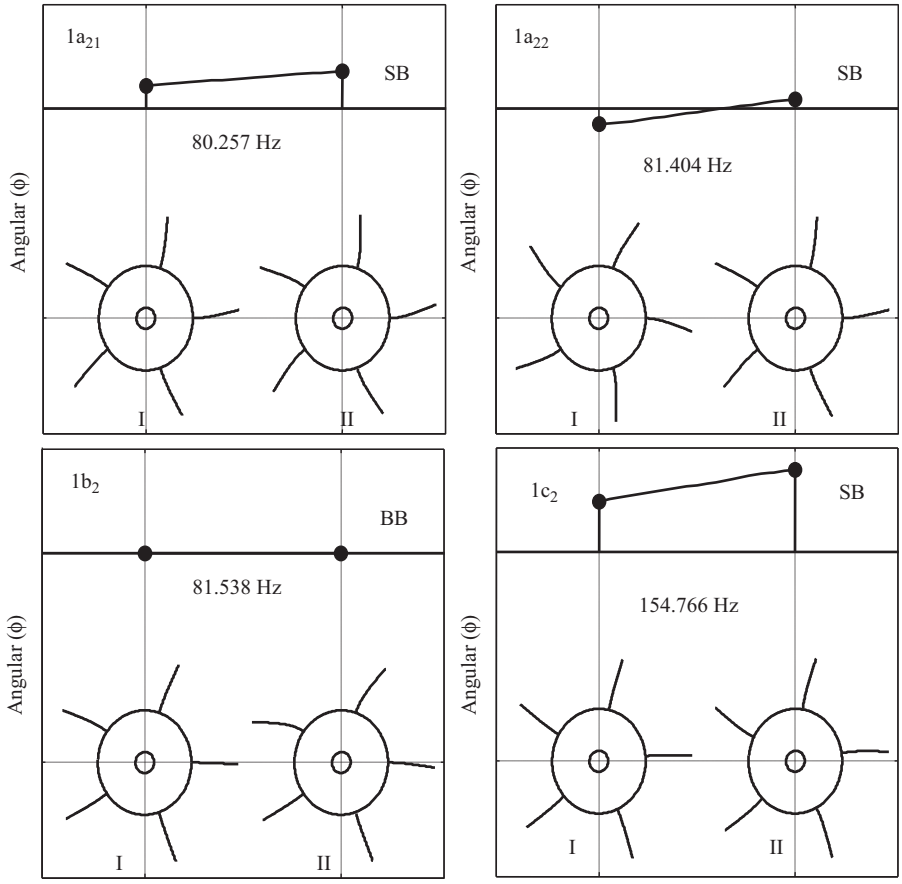

Fig. 6. The first four modes of the two-disks and five-blades rotor.

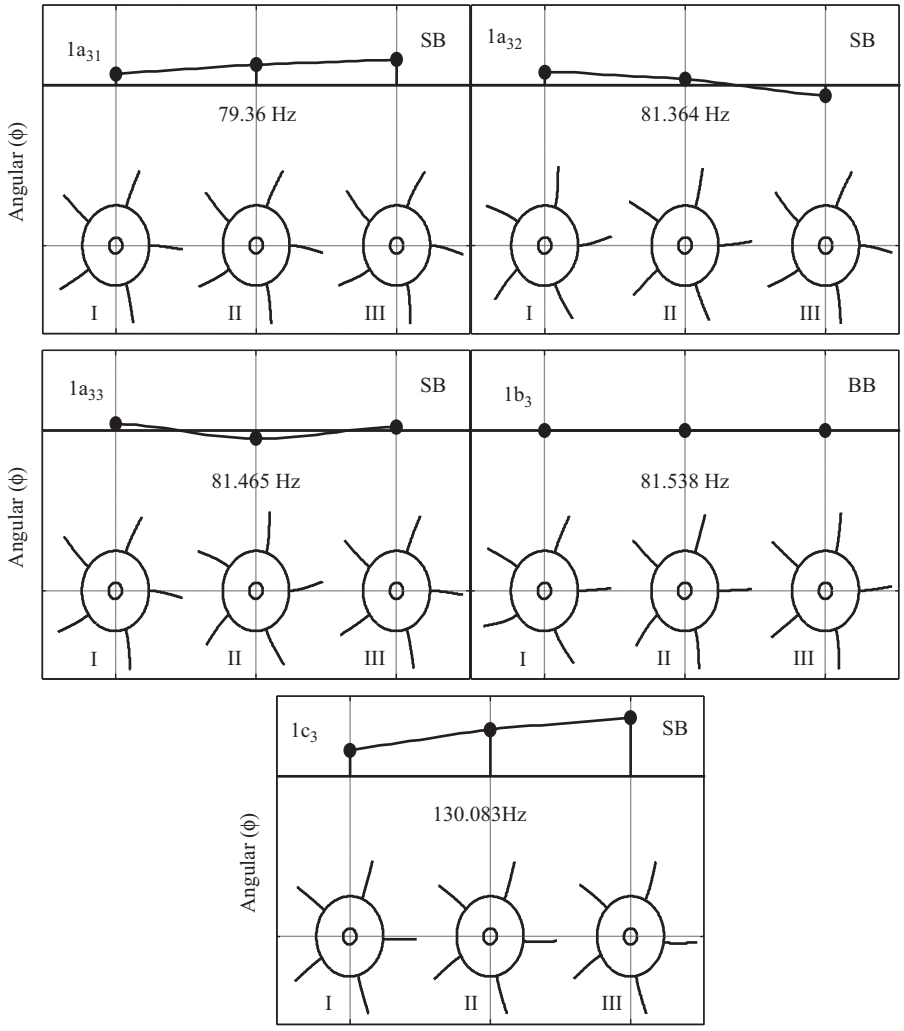

Fig. 7. The first five modes of the three-disks and five-blades rotor.

Figs. 5–7 show the modes where the blade's and shaft's first mode predominates of the five-blades for a one-disk to three-disk rotor.

Fig. 5 demonstrates the mode shapes of five-blade and one-disk case. The first line plot denotes the shaft's torsional displacement and the disk's and blade's deflection are illustrated in the following diagrams. Modes $1a_1$ and $1c_1$ have torsional displacements so that classified as SB modes. Fig. 6 shows five-blade and two-disk case. Compared to Fig. 5, it is seen that $1a_{21}$ and $1a_{22}$ modes are due to two-disk. Fig. 7 shows five-blade and three-disk case. Compared to Fig. 5, it is seen that $1a_{31}$, $1a_{32}$, and $1a_{32}$ modes are due to three-disk. That means the shaft–blade (SB) modes where the blade's mode predominates were of frequencies of N_d for number disks.

Fig. 8 illustrates how the frequency of the first three modes, varying with disks distance for a two-disks and five-blades rotor. Via the shaft–blade (SB) modes, $1a_{21}$ and $1a_{22}$ modes, it is seen that the frequency basically decreases with disks distance. From the figure, it is seen that the frequencies of $1a_{21}$ and $1a_{22}$ modes have 1% and 0.1% decrease from 0.2 to 2.0 with normalize disks distance.

The rotor's natural frequencies varying with rotation are illustrated. Figs. 9–11 plots the natural frequencies of a five-blade rotor. Fig. 9(a) shows, it is seen there exist frequency splits at each mode (as has been shown in Figs. 4 and 5). For the forward (positive) and backward (negative) frequencies approach to each other with the increase of rotation, two frequencies eventually merge and become one. At the merge point, the system implies a

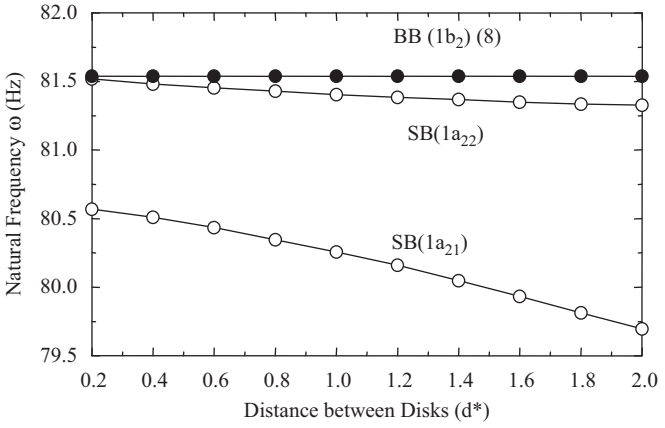

Fig. 8. $1a_{21}$, $1a_{22}$, and $1b_2$ modes frequency variations with disks distance for a two-disk and five-blade rotor.

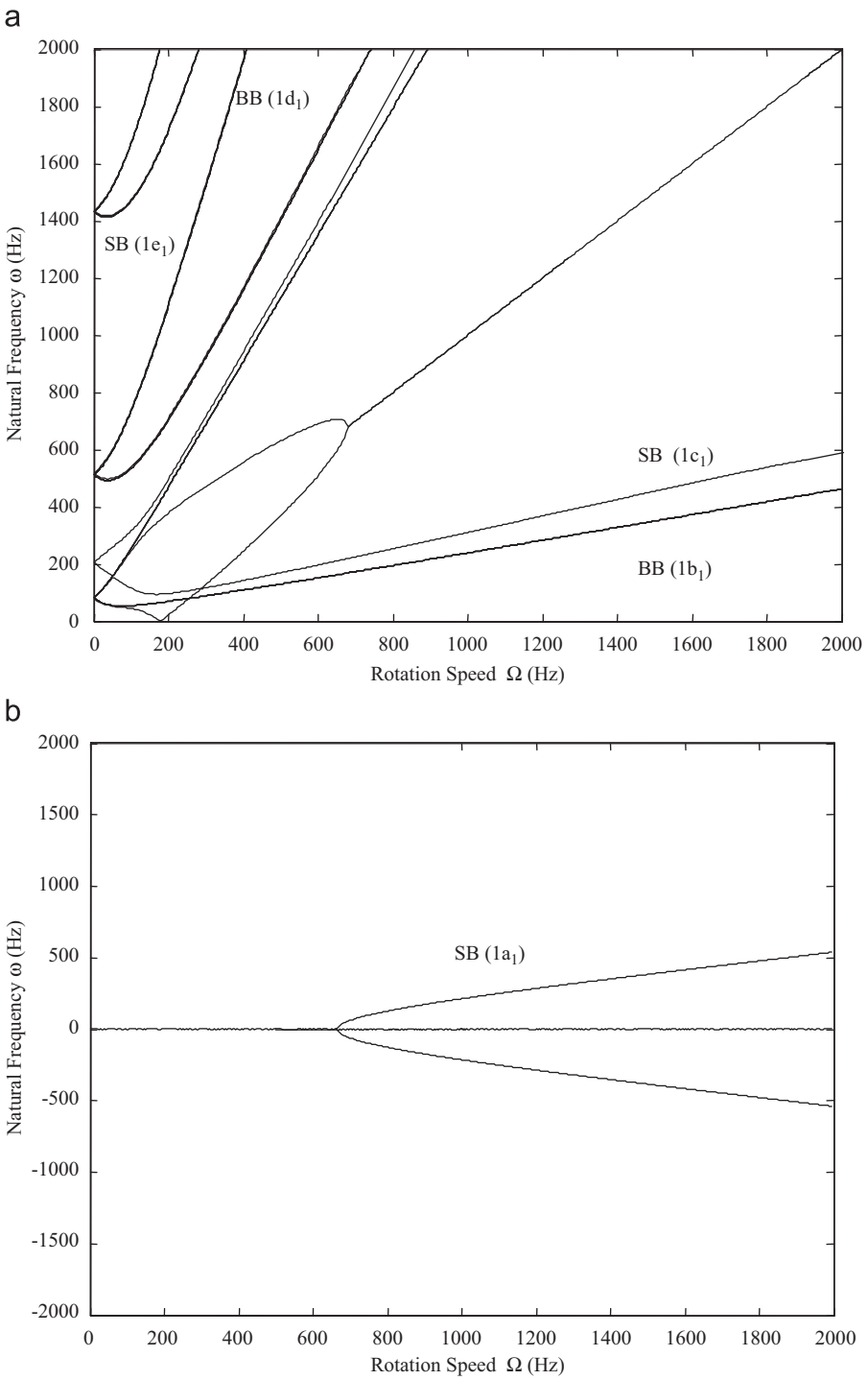

Fig. 9. Variation of eigenvalues with rotation speed for a one-disk and five-blade rotor.

possible instability. The authors adopted absolute value in y-axis in Fig. 9(a). Fig. 9(b) draws the real part of λ varying with rotation. It is seen that Re(λ) is zero before merging point, at which it becomes a pair of real numbers. It is seen that instability occurs at $1a_1$ mode is 650 Hz, but not for the others. Note that $1a_1$ mode is a SB mode. Fig. 10 shows two-disk case. Compared to Fig. 9, it is seen that $1a_{21}$ and $1a_{22}$ modes implies possible instability. At the merge point, the frequency of $1a_{21}$ mode is 450 Hz is earlier than $1a_1$ mode. Fig. 10 shows three-disk case. Compared to Fig. 9, it is seen that $1a_{31}$, $1a_{32}$, and $1a_{33}$ modes imply possible instability. At the merge point, the frequency of $1a_{31}$ mode is 400 Hz is earlier than $1a_1$ and $1a_{21}$ modes. Form the results it is seen that two important phenomena. First, a disk rotor implies a possible instability. Two-disk case causes two counts of possible instability, and so on. That means the times of instability will due to the number of disk. Second, the instability for three-disk case appears earlier than one- or two- disk case. In other words, it is seen that the more disk rotor causes instability earlier than the less disk case.

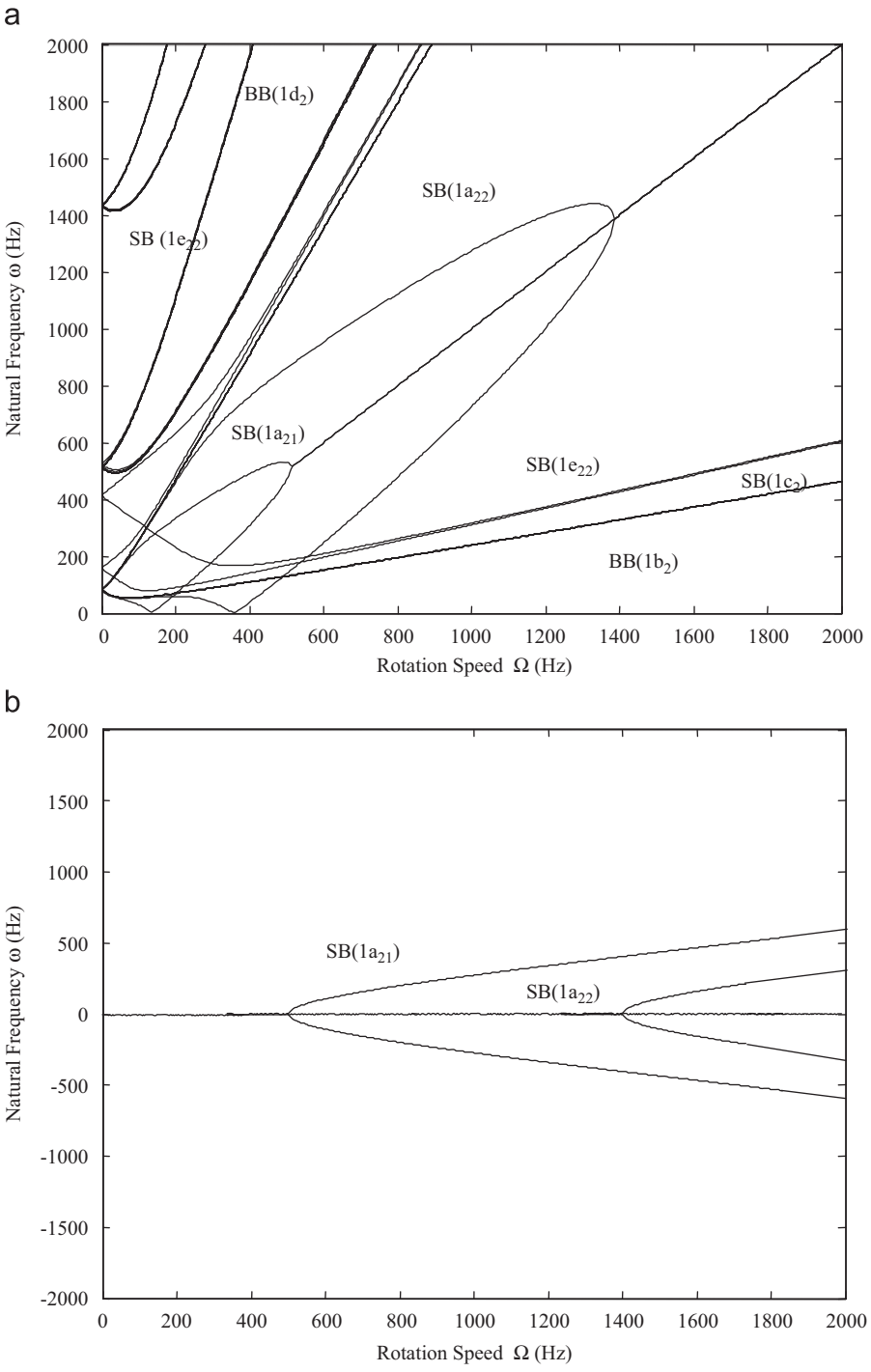

Fig. 10. Variation of eigenvalues with rotation speed for a two-disks and five-blades rotor.

4. Conclusion

This paper discussed the shaft-torsion and blade-bending coupling vibrations of a multi-disk rotor system. The assumed modes method was employed for the analysis.

The study began with the modes evolvement resulting from a disk. It is arrived at that the coupling modes could be grouped into two categories, the shaft–blade (SB) and blade–blade (BB). The BB modes were of repeated frequencies of (N_b-1) multiplicity for number blades.

A multi-disk system has drawn two important phenomena on the coupling modes. The SB modes added to N_d modes for number disks where the blade's mode predominates. The BB modes were of repeated frequencies of $[N_d \times (N_b-1)]$ multiplicity for number disks. Numerical calculation also revealed that the natural frequencies were affected by the disk distance.

As to rotation effects, the multi-disk has drawn two important phenomena. First, the times of instability will be due to the number of disk. Second, the more disk rotor causes instability earlier than the less disk case.

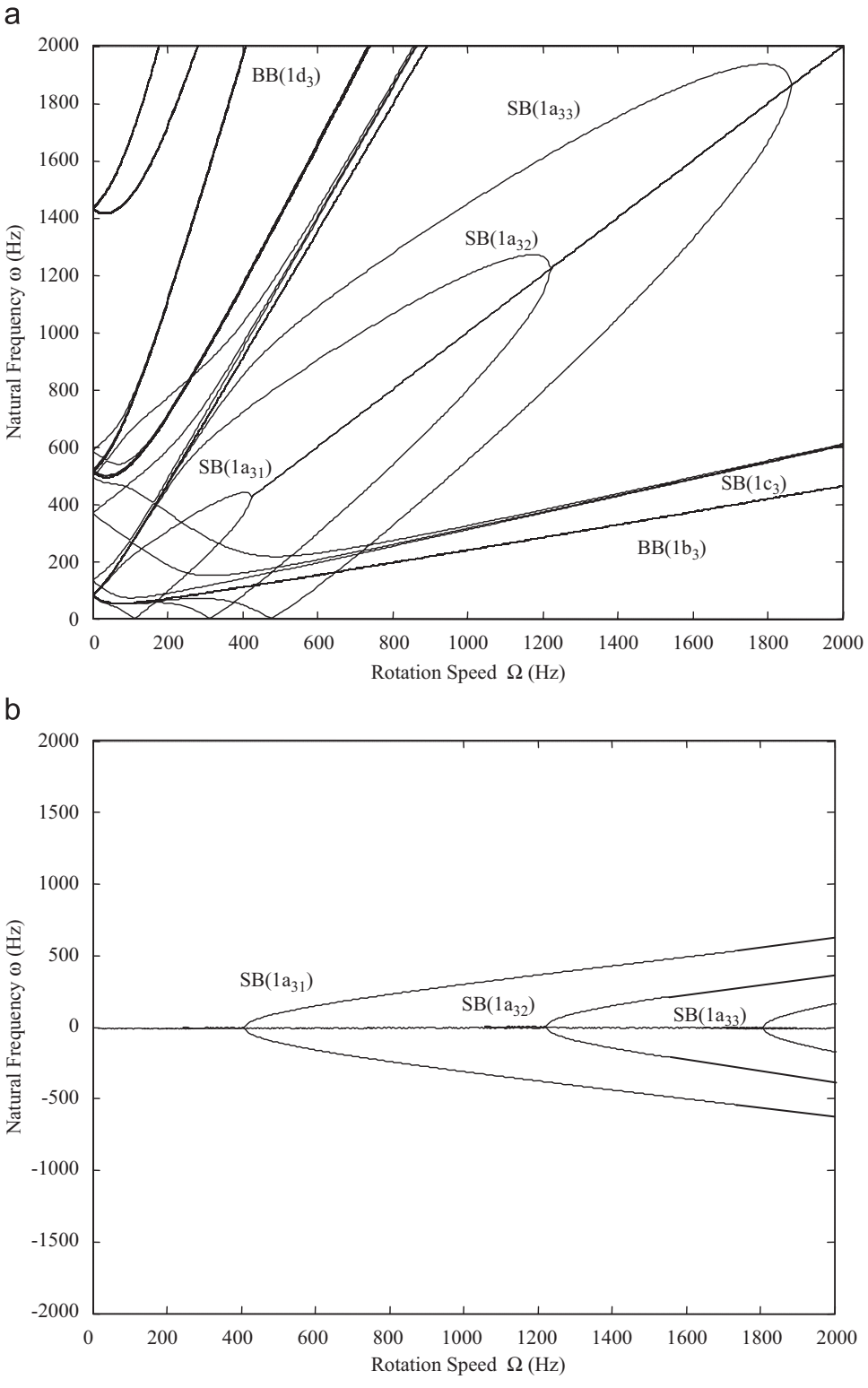

Fig. 11. Variation of eigenvalues with rotation speed for a three-disks and five-blades rotor.

Appendix A. Matrices elements

$$[\mathrm{M}]=\begin{bmatrix} [\mathrm{M}_s]_{n_s\times n_s} & [\mathrm{M}^1_{sb}]_{(n_s\times n_b)_1} & \cdots & [\mathrm{M}^{N_b}_{sb}]_{(n_s\times n_b)_1} & \cdots & [\mathrm{M}^1_{sb}]_{(n_s\times n_b)N_d} & \cdots & [\mathrm{M}^{N_b}_{sb}]_{(n_s\times n_b)N_d} \\ [\mathrm{M}^1_{sb}]^T_{(n_s\times n_b)_1} & [\mathrm{M}^1_b]_{(n_s\times n_b)_1} & [0]_{n_b\times n_b} & \cdots & \cdots & \cdots & \cdots & [0]_{n_b\times n_b} \\ \vdots & [0]^T_{n_b\times n_b} & \ddots & \ddots & \ddots & \ddots & \ddots & \vdots \\ [\mathrm{M}^{N_b}_{sb}]^T_{(n_s\times n_b)_1} & \vdots & \ddots & [\mathrm{M}^{N_b}_b]_{(n_s\times n_b)_1} & \ddots & \ddots & \ddots & \vdots \\ \vdots & \vdots & \ddots & \ddots & \ddots & \ddots & \ddots & \vdots \\ [\mathrm{M}^1_{sb}]^T_{(n_s\times n_b)N_d} & \vdots & \ddots & \ddots & \ddots & [\mathrm{M}^1_b]_{(n_s\times n_b)N_d} & \ddots & \vdots \\ \vdots & \vdots & \ddots & \ddots & \ddots & \ddots & \ddots & [0]_{n_b\times n_b} \\ [\mathrm{M}^{N_b}_{sb}]^T_{(n_s\times n_b)N_d} & [0]^T_{n_b\times n_b} & \cdots & \cdots & \cdots & \cdots & [0]^T_{n_b\times n_b} & [\mathrm{M}^{N_b}_b]_{(n_s\times n_b)N_d} \end{bmatrix} \tag{A.1}$$

$$[\mathrm{K}^e]=\begin{bmatrix} [\mathrm{K}^e_s]_{n_s\times n_s} & [0]_{n_s\times n_b} & \cdots & \cdots & \cdots & \cdots & \cdots & [0]_{n_s\times n_b} \\ [0]^T_{n_b\times n_s} & [\mathrm{K}^{e1}_b]_{(n_b\times n_b)_1} & [0]_{n_b\times n_b} & \cdots & \cdots & \cdots & \cdots & [0]_{n_b\times n_b} \\ \vdots & [0]^T_{n_b\times n_b} & \ddots & \ddots & \ddots & \ddots & \ddots & \vdots \\ \vdots & \vdots & \ddots & [\mathrm{K}^{eN_b}_b]_{(n_b\times n_b)_1} & \ddots & \ddots & \ddots & \vdots \\ \vdots & \vdots & \ddots & \ddots & \ddots & \ddots & \ddots & \vdots \\ \vdots & \vdots & \ddots & \ddots & \ddots & [\mathrm{K}^{e1}_b]_{(n_b\times n_b)N_d} & \ddots & \vdots \\ \vdots & \vdots & \ddots & \ddots & \ddots & \ddots & \ddots & [0]_{n_b\times n_b} \\ [0]^T_{n_b\times n_s} & [0]^T_{n_b\times n_b} & \cdots & \cdots & \cdots & \cdots & [0]^T_{n_b\times n_b} & [\mathrm{K}^{eN_d}_b]_{(n_b\times n_b)N_d} \end{bmatrix} \tag{A.2}$$

$$[\mathrm{K}^\Omega]=\begin{bmatrix} [\mathrm{K}^\Omega_s]_{n_s\times n_s} & [[\mathrm{K}^{\Omega 1}_{sb}]_{(n_s\times n_b)_1} & \cdots & [[\mathrm{K}^{\Omega N_b}_{sb}]_{(n_s\times n_b)_1} & \cdots & [[\mathrm{K}^{\Omega 1}_{sb}]_{(n_s\times n_b)N_d} & \cdots & [[\mathrm{K}^{\Omega N_b}_{sb}]_{(n_s\times n_b)N_d} \\ [[\mathrm{K}^{\Omega 1}_{sb}]^T_{(n_s\times n_b)_1} & [\mathrm{K}^{\Omega 1}_b]_{(n_b\times n_b)_1} & [0]_{n_b\times n_b} & \cdots & \cdots & \cdots & \cdots & [0]_{n_b\times n_b} \\ \vdots & [0]^T_{n_b\times n_b} & \ddots & \ddots & \ddots & \ddots & \ddots & \vdots \\ [[\mathrm{K}^{\Omega N_b}_{sb}]^T_{(n_s\times n_b)_1} & \vdots & \ddots & [\mathrm{K}^{\Omega N_b}_b]_{(n_b\times n_b)_1} & \ddots & \ddots & \ddots & \vdots \\ \vdots & \vdots & \ddots & \ddots & \ddots & \ddots & \ddots & \vdots \\ [[\mathrm{K}^{\Omega 1}_{sb}]^T_{(n_s\times n_b)N_d} & \vdots & \ddots & \ddots & \ddots & [\mathrm{K}^{\Omega 1}_b]_{(n_b\times n_b)N_d} & \ddots & \vdots \\ \vdots & \vdots & \ddots & \ddots & \ddots & \ddots & \ddots & [0]_{n_b\times n_b} \\ [[\mathrm{K}^{\Omega N_d}_{sb}]^T_{(n_s\times n_b)N_d} & [0]^T_{n_b\times n_b} & \cdots & \cdots & \cdots & \cdots & [0]^T_{n_b\times n_b} & [\mathrm{K}^{\Omega N_d}_b]_{(n_b\times n_b)N_d} \end{bmatrix} \tag{A.3}$$

$$[M_b]_{ij}=\rho_b A_b\int_{r_d}^{r_b} V_i V_j\,dx \tag{A.4}$$

$$[M_s]_{ij}=\int_0^{Ls} I_s\Phi_i\Phi_j\,dZ+I_d[\Phi_i\Phi_j]_{Z=Z_d}+\rho_b A_b\sum_1^{N_b}\int_{r_d}^{r_b} x^2[\Phi_i\Phi_j]_{Z=Z_d}\,dx \tag{A.5}$$

$$[M_{sb}]_{ij}=\rho_b A_b\int_{r_d}^{r_b} x\Phi_i|_{Z=Z_d} V_j\,dx \tag{A6}$$

$$[K^e_s]_{ij}=\int_0^{Ls} G_s J_s\Phi_i'\Phi_j'\,dZ \tag{A.7}$$

$$[K^e_b]_{ij}=E_b I_A\int_{r_d}^{r_b} V_i'' V_j''\,dx \tag{A.8}$$

$$[K^\Omega_s]_{ij}=\frac{1}{2}\rho_b A_b\sum_1^{N_b}\int_{r_d}^{r_b}(r_b^2-3x^2)[\Phi_i\Phi_j]_{Z=Z_d}\,dx \tag{A.9}$$

$$[K^\Omega_{sb}]_{ij}=\rho_b A_b\int_{r_d}^{r_b} x\Phi_i|_{Z=Z_d} V_j\,dx-\frac{1}{2}\rho_b A_b\int_{r_d}^{r_b}(r_b^2-x^2)\Phi_i|_{Z=Z_d} V_j'\,dx \tag{A.10}$$

$$[K^\Omega_b]_{ij}=\rho_b A_b\int_{r_d}^{r_b} V_i V_j\,dx-\frac{1}{2}\rho_b A_b\int_{r_d}^{r_b}(r_b^2-x^2)V_i' V_j'\,dx \tag{A.11}$$

References

[1] Bauer HF. Vibration of a rotating uniform beam part I: orientatation in the axis of rotation. Journal of Sound and Vibration 1980;72:177–89.

[2] Kammer Jr DC, Schlack AL. Effects of nonconstant spin rate on the vibration of a rotating beam. ASME Journal of Applied Mechanics 1987;54:305–10.

[3] Kammer Jr DC, Schlack AL. Dynamic response of a radial beam with non-constant angular velocity. ASME Journal of Vibration, Acoustics Stress, and Reliability in Design 1987;109:138–43.

[4] Pesheck E, Pierre C, Shaw SW. Modal reduction of a nonlinear rotating beam through nonlinear normal modes. Journal of Vibration and Acoustics 2002;124(2):229–36.

[5] Wang G, Wereley NM. Free vibration analysis of rotating blades with uniform tapers. AIAA Journal 2004;42(12):2429–37.

[6] Gunda JB, Singh AP, Chabbra. PPS, Ganguli R. Free vibration analysis of rotating tapered blades using Fourier-p superelement. Structures Engineering and Mechanics 2007;27(2):243–57.

[7] Gund JB, Gupta RK, Ganguli R. Hybrid stiff-string-polynomial basis functions for vibration analysis of high speed rotating beams. Computers and Structures 2009;87(3):254–65.

[8] Lee SY, Lin SM, Lin YS. Instability and vibration of a rotating beam with precone. International Journal of Mechanical Sciences 2009;51(2):114–21.

[9] Gunda JB, Ganguli. R. Stiff string basis function for vibration analysis of high speed rotating beams. Journal of Applied Mechanics 2009;75(2):0245021–5.

[10] Shen IY. Closed-form forced response of a damped, rotating, multiple disks/spindle system. ASME Journal of Applied Mechanics, Transactions 1997;64:343–52.

[11] Shen IY, Ku CPR. Nonclassical vibration analysis of a multiple rotating disk and spindle assembly. ASME Journal of Applied Mechanics, Transactions 1997;6(1):165–74.

[12] Khorasany MH, Hutton. SG. An analytical study on the effect of rigid body translational degree of freedom on the vibration characteristics of elastically constrained rotating disks. International Journal of Mechanical Sciences 2010;52(9):1186–92.

[13] Nevzat OH. On the critical speed of continuous shaft–disk systems. Journal of Vibration, Acoustics, Stress, and Reliability in Design 1984;106:59–61.

[14] Wu F, Flowers. GT. A transfer matrix technique for evaluating the natural frequencies and critical speeds of a rotor with multiple flexible disk. ASME Journal of Vibration and Acoustics 1992;114:242–8.
[15] Chun SB, Lee CW. Vibration of shaft-bladed disk system by using substructure synthesis and assumed modes method. Journal of Sound and Vibration 1996;189:587–608.
[16] Omprakash V, Ramamurti V. Coupled free vibration characteristics of rotating tuned bladed disk systems. Journal of Sound and Vibration 1990;140: 413–35.
[17] Lesaffre N, Sinou JJ, Thouverez F. Contact analysis of a flexible bladed-rotor. European Journal of Mechanics A/Solids 2007;26:541–57.
[18] Huang SC, Ho KB. Coupled shaft-torsion and blade-bending vibration of a rotation shaft–disk–blade unit. ASME Journal of Engineering for Gas Turbines and Power 1996;118:100–6.
[19] Yang CH, Huang SC. Coupling vibration in rotating shaft–disk–blades system. ASME Journal of Vibration and Acoustics 2007;129:48–57.
[20] Yang CH, Huang SC. The longitudinal motion effects on the coupled vibration in a shaft–disk–blades system. Journal of Chinese Institute Engineers 2004;28: 89–99.
[21] Yang CH, Huang SC. The influence of disk's flexibility on coupling vibration of shaft–disk–blades systems. Journal of Sound and Vibration 2007;301:1–17.
[22] Huang SC, Chiu YJ, Lu YJ. Damping property and vibration analysis of blades with viscoelastic layers. Journal of System Design and Dynamics 2007;1: 340–51.
[23] Chiu YJ, Huang SC. Shaft-torsion and blade-bending coupling vibrations in a rotor system with grouped blades. Journal of System Design and Dynamics 2007;1:748–59.